Factors Influencing the Surface Functionalization of Citrate Stabilized Gold Nanoparticles with Cysteamine, 3-Mercaptopropionic Acid or L-Selenocystine for Sensor Applications

Georgia I. Sakellari [1,†] , **Nicole Hondow** [2] **and Philip H.E. Gardiner** [1,*]

1   Biomolecular Sciences Research Centre, Sheffield Hallam University, Sheffield S1 1WB, UK;
    Jo.Sakellari@warwick.ac.uk
2   School of Chemical and Process Engineering, University of Leeds, Leeds LS2 9JT, UK;
    N.Hondow@leeds.ac.uk
*   Correspondence: p.h.gardiner@shu.ac.uk
†   Present address: School of Chemical Engineering, University of Birmingham, Birmingham B15 2TT, UK.

check for
updates

Abstract: Thiols and selenides bind to the surface of gold nanoparticles (AuNPs) and thus provide suitable platforms for the fabrication of sensors. However, the co-existence of adsorbed citrate on the surface of the nanoparticles can influence their functionalization behavior and potentially their sensing performance measured by the extent of particle aggregation. In this study, the functionalization of purchased (7.3 ± 1.2 nm) and in-house prepared AuNPs (13.8 ± 1.2 nm), under the same experimental conditions with either cysteamine (Cys), 3-mercaptopropionic acid (3-MPA), or L-selenocystine (SeCyst) was investigated. ^{1}H-NMR measurements showed distinct citrate signatures on the in-house synthesized citrate-stabilized AuNPs, while no citrate signals were detected on the purchased AuNPs other than evidence of the presence of α-ketoglutaric acid. Carboxylate-containing species attributed to either citrate or α-ketoglutaric acid were identified in all functionalized AuNPs. ATR-FTIR spectroscopy confirmed the functionalization of AuNPs with Cys and 3-MPA, and energy dispersive X-ray (EDX) spectroscopy measurements suggested the formation of SeCyst functionalized AuNPs. Co-adsorption rather than displacement by the functionalizing agents and carboxylate-containing molecules was indicated, which for Cys and SeCyst functionalized AuNPs was also the aggregation limiting factor. In contrast, the behavior of 3-MPA functionalized AuNPs could be attributed to electrostatic repulsions between the functionalized groups.

Keywords: gold nanoparticles; cysteamine; 3-Mercaptopropionic Acid; L-Selenocystine; functionalization; self-assembled monolayers; sensor applications

1. Introduction

Gold nanoparticles possess unique chemical and physical properties, which can be harnessed for drug delivery [1,2], the development of sensors [3,4], biological imaging [5], and the detection of biomarkers [6], among other applications. More specifically, in sensor applications they have been deployed for chemical and biological sensing [7,8], diagnostics [9] and more recently in environmental monitoring [10,11] because AuNPs based sensors can be fabricated with the potential to detect a wide variety of molecules (organic and inorganic), proteins, cancerous cells and metal ions. The key properties of AuNPs include electronic, magnetic and optical characteristics, with the latter arising from localized surface plasmon resonance (LSPR), which is the collective effect of the oscillations of free electrons at the surface of the metal [12]. Gold nanoparticles are rich in conduction electrons,

which can be easily polarized under the influence of an electromagnetic field to produce non-linear optical phenomena [13]. Self-assembled monolayers (SAMs) have been used to modify the surface of gold nanoparticles, as they influence the stability of the colloidal solution, and provide the platform on which the reactivity of the particles can be altered [14]. Changes in the SPR band can be used to determine whether functionalization of the AuNPs has occurred, while the effects of such changes can provide information on the nature of the interactions between the particles [15,16]. Exploitation of these interactions can be used in the design of SAMs with different functional groups, which offer platforms that can selectively interact with appropriate analytes, resulting in the development of highly sensitive and versatile colorimetric sensors.

In the last few years, gold nanoparticles have been commercially available in a range of sizes (5–250 nm), and dispersed in a variety of stabilizers such as citrate buffer, phosphate-buffered saline (PBS), H_2O and D_2O [17–19]. Published literature is replete with studies in which different preparation methods have been used to produce AuNPs in a variety of shapes, sizes, and in different stabilization media [20–22]. However, the deployment of a myriad of preparation methods makes it difficult to compare results from different studies, particularly when little attention is paid to the impact of the experimental conditions on the surface behavior of the synthesized AuNPs. Only recently, a study by Havaldar et al. [23] compared the functionalization behavior of AuNPs prepared following three different preparation methods, where it was suggested that the citrate-stabilized AuNPs prepared with the Turkevich et al. [17] method did not show any potential for conjugation with any of the 22 ʟ-amino acids that were used. Conversely, the particles synthesized using plant-mediated and bacteria-mediated methods were more suitable for functionalization, highlighting for the first time the effect of the synthetic method on the surface properties of the AuNPs. The in situ synthesis introduced by Turkevich et al. [17] is one of the most frequently used methods for production of citrate-stabilized AuNPs with sizes of about 20 nm. Over the years, a plethora of modifications have been made to this method to obtain AuNPs of different sizes (15–150 nm) by altering the trisodium citrate to $HAuCl_4$ ratio [24], changing the pH of the solution [25], controlling the reaction temperature [26], adding the use of fluorescent light irradiation [27] or high-power ultrasound [28], and substituting water with D_2O as the solvent [18]. However, it has been suggested that increasing the citrate concentration could result in unstable nanoparticles overtime [29], while adjusting the pH can have a significant effect on the size distribution and potentially on the shape of the particles [30]. In a study following the method proposed by Turkevich et al. [17] it was shown that decreasing the molar ratio between citrate and gold during synthesis, the size of the particles increased, while they became more polydisperse and less spherical [31].

One of the most extensively studied methods to alter the surface properties of gold nanoparticles has been the use of SAMs based on sulfur, due to their binding affinity for the surface of gold. Selenium-based SAMs are to be preferred to those of sulfur because of their bonding preference and higher packing density on gold compared to thiol monolayers [32,33]. As regards the classical method used for the production of AuNPs by citrate reduction and subsequent stabilization by the anion, there is now evidence to suggest that not all of the citrate is displaced from the surface of gold upon functionalization with thiols [34,35]. Wei et al. [36] monitored the kinetics of citrate desorption from the surface of AuNPs and showed that thiol-containing molecules were the most efficient at displacing citrate compared to amine- and carboxylate-containing molecules, but without complete displacement. The explanation for this observation was attributed to different binding energies of citrate on the gold surface. In contrast, Perera et al. [37] have demonstrated that citrate residues can be displaced by thiols from the surface of AuNPs. Similarly, in a study using gold nanoparticles in thio-compound nanomedicine, citrate was displaced by the thiol-based drug thioabiraterone, which displayed interaction with the AuNPs [38]. In another study [39], the ability of three amino acids cysteine, arginine and glutamic acid to replace citrate from the surface of AuNPs was assessed, and it was demonstrated that cysteine containing a thiol functional group was the most effective at replacing citrate. These contradictory findings illustrate the importance of establishing the effect of the presence

of the adlayer of citrate or solution contaminants on the functionalization behavior of synthesized AuNPs using both thiolates and selenides. Employing nanoparticles produced following procedures which meet certain standards, would allow better comparison of the results between different research investigations, and at the same time would ensure the quality and consistency of the observations.

Herein the conditions for the functionalization of citrate-stabilized gold nanoparticles with the short chain aliphatic compounds: cysteamine (Cys), 3-mercaptopropionic acid (3-MPA) and L-selenocystine (SeCyst), respectively are investigated. The selection of these thiolate and diselenide compounds, which are of great interest for their utilization in SAMs, was based on their ability to provide platforms that can be utilized to link their terminal groups with other structures, thus producing materials with desirable properties for sensor applications. Two types of citrate-stabilized AuNPs were chosen; a purchased solution and an in-house synthesized based on a slightly modified version of the Turkevich method [20]. The functionalization and purification methods were kept the same for both types of AuNPs, in order to assess the effect of the solution characteristics on the functionalization behavior. The presence of adsorbed citrate or other species on the surface of purchased and in-house prepared gold nanoparticles that could potentially affect the extent to which the particles are functionalized was investigated. For this purpose, UV-vis spectroscopy, ^{1}H nuclear magnetic resonance (^{1}H-NMR), attenuated total reflectance-Fourier-transform infrared (ATR-FTIR), and transmission electron microscopy (TEM) measurements were employed.

2. Experimental Section

2.1. Materials and Methods

The following reagents and materials were all purchased from Sigma-Aldrich Co., Ltd. (Gillingham, UK): gold nanoparticles (AuNP) stabilized suspension in citrate buffer (stated average diameter, 10 nm), cysteamine hydrochloride ($NH_2CH_2CH_2SH$, ≥98%), HEPES buffer sodium salt (0.01 M), sodium bicarbonate (≥99.7%), hydrochloric acid (reagent grade, 37%), nitric acid (ACS reagent 70%), deuterium oxide deuteration degree min. 99.96% for NMR spectroscopy, L-selenocystine ($CO_2HCH(NH_2)CH_2(Se)_2CH_2CH(NH_2)CO_2H$, 95%), 3-mercaptopropionic acid ($HSCH_2CH_2CO_2H$, ≥99%), phosphate buffer solution (1.0 M, pH 7.7), gold standard for ICP (1000 mg/L Au in hydrochloric acid), hydrogen tetrachloroaurate (III), $HAuCl_4.3H_2O$, 99.99% pure, sodium hydroxide solution (0.05 M, ≥97%), sodium citrate monobasic, $HOC(COONa)(CH_2COOH)_2$, ≥99.5%. Trisodium citrate dihydrate, $Na_3C_6H_5O_7.2H_2O$, 99% was purchased from Fischer Scientific (Loughborough, UK).

2.2. Synthesis and Characterization of Citrate-Capped AuNPs

All glassware was washed in aqua regia (3:1 HCl:HNO$_3$), rinsed with deionized water, and then oven-dried prior to use. Citrate-stabilized AuNPs were prepared using citrate reduction of HAuCl$_4$ [20]. Briefly, HAuCl$_4$ (100 mL, 0.506 mM) was brought to the boil under vigorous stirring, and then trisodium citrate dihydrate (10 mL, 19.4 mM, pH 8.5) was quickly added. The color of the solution turned from light yellow to colorless, black and finally wine red. After boiling and stirring for 10 min, the solution was set aside and allowed to cool to room temperature, followed by filtering through a 0.22 μm pore diameter syringe filter (Merck Millipore, Watford, UK) to remove any large particulates. The resulting solution was stored in the dark at 4 °C until required. The UV-vis absorption spectrum showed that λ_{max} the peak maximum of the SPR band was at 520 nm. Transmission electron microscopy (TEM) indicated that the average size of the formed nanoparticles was 13.8 ± 1.2 nm. Inductively coupled plasma optical emission spectroscopy (ICP-OES) analysis was performed to determine the concentration of the synthesized AuNPs, and was found to be 10.80 mg L^{-1} (0.055 mM).

The purchased AuNPs used in this study were acquired from Sigma-Aldrich Co., Ltd. According to the information supplied, the solution was characterized by a core size range of 8–12 nm (average diameter of 10 nm) and an absorption maximum of 510–525 nm, stabilized in citrate buffer. The measured absorbance maximum was 524 nm, and the concentration of gold in the solution determined by ICP-OES

was 60.3 ± 0.2 mg L^{-1} or (0.307 mM). This result corresponds to an average nanoparticle diameter of 8 nm, which was confirmed by TEM measurements indicating an average diameter of 7.3 ± 1.2 nm.

2.3. Modification and Purification of Cysteamine, 3-Mercaptopropionic Acid and L-Selenocystine Capped AuNPs

For the functionalization of the AuNPs with either cysteamine (Cys), 3-mercaptopropionic acid (3-MPA) or L-selenocystine (SeCyst), solutions of varying molarities (0.256, 0.506, 1.012, 2.024, 3.036, 4.048 and 5.06 mM) of the three compounds were prepared in different dissolution media. The media used were deionized water, D_2O, HEPES buffer (0.01 M, pH 9.7) and phosphate buffer (0.01 M, pH 7.7). Functionalization was performed in 96-well plates, by adding 50 µL of AuNPs and 50 µL of each of the functionalizing agents, dissolved in any of the chosen dissolution media. To obtain a final volume of 1 mL for each solution, which would undergo purification or any later analyses, 10 wells were used each time. Stability assessment of the colloids was performed for all solutions and at various pH values after adjustment with either HCl or NaOH. During preliminary studies, optimization of the stability conditions was performed using the purchased AuNPs, which were subsequently used for the modification of both purchased and synthesized AuNPs. The conditions were kept the same to ensure that any disparity in the observations was not caused by differences in the methods followed. UV-vis measurements of the colloidal solutions were obtained after 2 h and overnight incubation at 4 °C. All samples were stored in the dark.

The modified gold nanoparticles were purified by removing the excess un-adsorbed functionalizing agents (Cys, 3-MPA or SeCyst) before any measurements. After overnight incubation at 4 °C, excess reagents were removed by a cycle of centrifugation using open-top thick wall propylene tubes (TLA-120.2, Beckman Coulter, Brea, CA, USA). 1 mL aliquots of the samples was initially centrifuged at 22,000 rpm for 40 min at 4 °C, the supernatant was carefully removed and 500 µL of phosphate buffer (pH 7.7) was added. The pellets were re-suspended in phosphate buffer after sonication at room temperature for 5 min, and the resulting colloidal solution was then centrifuged at 22,000 rpm for 40 min at 4 °C. Lastly, after removing the supernatant, the precipitate was freeze dried and kept in the freezer for subsequent analyses. The above speeds and times were experimentally optimized, in order to avoid aggregation or the production of tight pellets.

2.4. Characterization of AuNPs Capped with Different Agents

The UV-vis absorption spectra of the samples were recorded using a microplate reader (Infinite M200, Tecan, San Francisco, CA, USA) in Nunclon transparent 96 well microplates (Thermo Scientific, Hempstead, UK), to obtain information about the position and shape of the LSPR band, before and after the various modifications (e.g., functionalization of the AuNPs). Attenuated total reflectance-Fourier-transform infrared (ATR-FTIR) spectra were obtained using a PerkinElmer spectrum 100 FTIR spectrometer (PerkinElmer, Waltham, CA, USA) equipped with a universal ATR (UATR) accessory. The samples were lyophilized prior to analysis. FTIR results were used to study the conjugation of the AuNP surface. [1]H nuclear magnetic resonance (^{1}H-NMR) spectra were recorded on an AVANCE III (400 MHz) NMR spectrometer (Bruker, Billerica, MA, USA) to assess the functionalization and characterize the composition of the synthesized and purchased AuNP solutions. All samples were freeze dried overnight and re-suspended in D_2O before analysis. Inductively coupled plasma optical emission spectroscopy (ICP-OES) analyses were performed on an ACTIVA M ICP-OES spectrometer (HORIBA Jobin Yvon IBH Ltd., Glasgow, UK), in order to determine the concentration of gold in the purchased and synthesized AuNP solutions. Appropriate volumes of Au standard to give concentrations of 0, 5, 10, 15 and 20 mg L^{-1} were transferred into 100 mL volumetric flasks, 1 mL of aqua regia was added in each sample, and the volume was made up to mark with deionized water. The synthesized and purchased AuNP samples were prepared by digestion of 1 mL of each solution with equal volume of aqua regia for 30 min, and then the volume was made up to 10 mL. All samples were analyzed in triplicates, at two wavelengths: 242.795 and 267.595 nm. Inductively

coupled plasma mass spectrometry (ICP-MS) measurements were obtained on a NexIon 350X ICP-MS tuned using a NexIon Setup Solution (Perkin Elmer, Buckinghamshire, UK). Semi-quantitative analysis was performed to assess whether the re-suspension of gold in the supernatant had occurred after the centrifugation of the AuNPs. The following Au standards: 0, 0.1 and 1 mg L^{-1} were prepared in deionized water. Transmission electron microscopy (TEM) measurements were carried out to investigate the size, shape, and confirm the surface modification of the nanoparticles. For the analysis, a few drops of methanol were added to vials of dried samples, and after sonication a drop was placed on a copper TEM grid coated in a continuous carbon film. Following drying, the samples were examined with a FEI Titan^3 Themis G2 S/TEM (FEI company, Hillsboro, OR, USA) operating at 300 kV fitted with four energy dispersive X-ray (EDX) silicon drift detectors, a Gatan Quantum ER energy filter (Gatan Inc, Pleasanton, CA, USA) and a Gatan One-View CCD. The size distribution analysis was performed using ImageJ analysis software. Energy-dispersive X-ray (EDX) spectroscopy and mapping was undertaken using Bruker Esprit v1.9 software, and electron energy loss spectroscopy (EELS) were collected and analyzed using Gatan Digital Micrograph V3.01.

3. Results and Discussion

3.1. Surface Characterization of Citrate-Stabilized AuNPs

UV-vis spectra of the purchased and in-house synthesized AuNPs showed absorption maximum (λ_{max}) at 524 and 520 nm, respectively. Comparison of the extinction spectra and physical appearance between the two solutions is provided in the Supplementary Materials (Figure S1). The SPR band of the synthesized AuNPs solution has higher absorbance and is sharper compared to the purchased AuNPs. The disparity in the absorbance maxima could be attributed to the difference between the average nanoparticle diameter of the purchased (7.3 ± 1.2 nm) (Figure S2) and synthesized AuNPs (13.8 ± 1.2 nm) (Figure S3) [40–42].

^{1}H-NMR spectra were acquired for both AuNP samples in order to compare their composition, identify the compounds present, and confirm the successful formation of citrate-stabilized gold nanoparticles (Figure S3). The AuNPs in the two suspensions were washed before analysis following the purification method described above, freeze dried overnight and re-suspended in D_2O. The spectra of the two AuNP solutions showed differences. However, there were a few peaks present in both the synthesized AuNPs (Figure S4A), and the trisodium citrate solution (Figure S5). A summary of the ^{1}H-NMR spectral features in the three solutions is provided in Table 1.

Table 1. ^{1}H-NMR data for synthesized, purchased AuNPs and trisodium citrate.

Chemical Shift (ppm)	Pattern	Coupling Constant *J* (Hz)	Assignment	Samples
3.44	singlet	-	Acetoacetic acid	Synthesized AuNPs
2.59, 2.55	doublet	15	Citrate	Synthesized AuNPs, trisodium citrate
2.47, 2.44	doublet	12	Citrate	Synthesized AuNPs, trisodium citrate
2.74, 2.70	doublet	15	Other "forms" of citrate [43]	Trisodium citrate
2.30, 2.26	doublet	15	Other "forms" of citrate	Trisodium citrate
2.14	singlet	-	Acetone	Synthesized AuNPs, trisodium citrate
1.82	singlet	-	Acetic acid	Synthesized AuNPs, purchased AuNPs
3.67, 3.65, 3.63	triplet	8, 8	α-ketoglutaric acid	Purchased AuNPs
3.056, 3.044, 3.036, 3.026, 3.015	quintet	4.8, 3.2, 4, 4.4	-	Purchased AuNPs
2.758, 2.747, 2.738, 2.730, 2.717	quintet	4.4, 3.6, 3.2, 5.2	-	Purchased AuNPs
2.54, 2.52, 2.51	triplet	6, 6	α-ketoglutaric acid	Purchased AuNPs
1.19	singlet	-	-	Purchased AuNPs

The AB system of citrate was observed around 2.5 ppm in the spectra of the synthesized AuNPs and trisodium citrate solutions, but it was absent from the purchased AuNPs suspension, which displayed a broad triplet at 2.5 ppm. The signals of acetone (2.14 ppm), acetic acid (1.82 ppm) and acetoacetic acid (3.44 ppm) which are products of intermediate reactions during the oxidation of citrate in the formation

of AuNPs, can be identified in the synthesized AuNPs solution (Figure S4A). It is noteworthy that the peaks observed in the spectrum of the synthesized solution were broader and less intense compared to the spectrum of trisodium citrate, since the species are adsorbed onto the nanoparticles, and are also present at much lower concentrations. The spectrum of the trisodium citrate solution contained two additional doublets at the foot of the citrate signals centred at 2.70 ppm and 2.30 ppm (Figure S5). These two doublets, along with two shoulders at 2.68 ppm and 2.38 ppm on the large citrate signals suggest the presence of two other "forms" of citrate [43]. However, these peaks were absent from the spectrum of the synthesized NPs, indicating the presence of only one form of citrate adsorbed on the surface of the AuNPs. In the case of the purchased AuNPs, confirmation of the solution content was not possible since there was no other information provided by the supplier, apart from the identity of the stabilizing agent. However, the two triplets around 3.6 and 2.5 ppm could be assigned to the presence of α-ketoglutaric acid, which was previously identified in another study [44]. Acetic acid was present in both AuNP solutions, while the characteristic peaks of citrate were not identified in the purchased AuNPs solution. ^{1}H-NMR results show that the species found in both solutions are different, with no identifiable citrate peaks in the purchased AuNPs solution.

ATR-FTIR spectroscopy measurements were also carried out on the lyophilized samples, in order to obtain additional information on the composition of the AuNPs solutions and confirm the formation of citrate-stabilized AuNPs (Figure S6). The ATR-FTIR results are summarized in Table S1. The successful removal of excess amount of citrate in the solution was ensured by washing the samples once with phosphate buffer at a pH that would not cause them to aggregate (pH 7.7), and then using D_2O to minimize the interference effect of H_2O. The spectrum of trisodium citrate dihydrate was obtained as a reference (Figure S7). The transmittance level of the peaks in the AuNPs spectra was lower compared to that of the pure citrate solution, due to the lower concentrations of citrate present in these samples. The broad peak around 3200 cm^{-1} assigned to free v(O-H)$_{COOH}$ stretching vibration was identified in all three solutions. The two peaks at 2918 cm^{-1} and 2850 cm^{-1} were associated with v(C-H) stretching vibration and were only found in the synthesized AuNP solutions. These peaks were present under basic conditions and assigned to the methylene groups of citrate attached on the surface of the nanoparticles [34]. The peak at 1732 cm^{-1} was observed only in the purchased AuNP solution and could be attributed to a non-interacting -COOH group on the surface of the AuNPs [45]. The peak around 1660 cm^{-1} (Figure S6A,B) could correspond to v_{asy}(COO$^-$) vibration, previously described as hydrogen bond formation between carboxyl groups [46]. The peak at 1560 cm^{-1} assigned to v_{asy}(COO$^-$) stretching vibration was slightly shifted in the synthesized AuNPs solution, indicating the presence of an intramolecular hydrogen bond with a -OH group. The peak at 1386 cm^{-1} in the citrate solution was attributed to another v(COO$^-$) band stretching vibrational mode that was slightly shifted in the AuNPs spectrum. The alcohol group stretching vibrational mode v_{asy}(C-O)$_{alch}$ band was detected in the citrate solution at 1138 cm^{-1}, and was also present in all three spectra at 1078, 1080, and 1087 cm^{-1}, with a small shift in the Cit-AuNPs sample. The peak shift in the Cit-AuNPs spectra, as well as the appearance of peaks absent from the pure trisodium citrate solution suggest the successful formation of citrate-stabilized AuNPs.

Both the ^{1}H-NMR and ATR-FTIR results show that the pre-treatment protocol developed here could not remove entirely the citrate bound to the surface of the synthesized AuNPs. There is now evidence that not all of the citrate bound on the AuNPs surface is easily displaced. As the density of the citrate is reduced when the monodentate bound citrate species are displaced, binding of the remainder is transformed to the more tightly bound dicarboxylate bridging form. Detailed discussion on the nature of the association between citrate and the gold surface can be found in articles by Park and Shumaker-Parry [34,45]. The effect of the surface bound citrate on the functionalization of the AuNPs by Cys, 3-MPA and SeCyst, respectively is shown and discussed below.

3.2. Optimization of the Conditions for the Functionalization of Citrate-Stabilized AuNPs

The conditions under which the functionalization of the AuNPs occurred were optimized, and the parameters considered included the dissolution of the compounds, the concentration of the compounds, the pH of the solution, and the centrifugation settings (Table S2). This was necessary not only to establish the conditions for the functionalization of the AuNPs, but also to study the long-term stability of the colloidal solutions. For this purpose, purchased AuNPs were used, and then the optimum conditions were applied to the functionalization of both the purchased and synthesized AuNPs. In order to select the optimum ratio between the AuNPs and the functionalizing agents, a range of solutions with different concentrations of cysteamine, 3-mercaptopropionic acid and L-selenocystine were prepared. These concentrations were based on theoretical calculations for the concentration of gold in the purchased solution assuming the mean diameter of 10 nm of the AuNPs, as suggested in the product information. The calculated concentration of gold in the solution was 0.506 mM. On this basis, the solutions were prepared in the following concentrations and ratios of functionalizing agent/HAuCl$_4$: 0.256 mM (1:2), 0.506 mM (1:1), 1.012 mM (2:1), 2.024 mM (4:1), 3.036 mM (6:1), 4.048 mM (8:1), 5.06 mM (10:1).

Effect of pH on Functionalization

It has been shown that the pH is a critical parameter for the stability of the colloidal solution, as it can cause changes in the electrostatic interactions between the particles [47]. Therefore the experiments were initially performed in sodium HEPES buffer adjusted at pH 7.4 to prevent aggregation of the AuNPs. Both thiol compounds showed good stability indicated by UV-visible spectroscopy, although the SPR band slightly broadened and there were bathochromic or red shifts of the peak maxima, the band shape remained unchanged after overnight incubation (Figure S8) [48]. For L-selenocystine, only the 1:2, 1:1 and 2:1 ratios were used for the functionalization of the AuNPs, as the higher ratios could not be dissolved in the HEPES buffer. The concentrations of SeCyst after the addition of an equal volume of AuNPs were: 0.128, 0.256 and 0.506 mM, respectively. This is in agreement with previous results suggesting that diselenides require a smaller amount to form well dispersed SAMs on gold nanoparticles, compared to thiolates [49]. Therefore, an additional ratio of 1:4 was prepared. The stability of the SPR bands in the solutions was assessed using the UV-vis absorption spectra of the solutions obtained after 2 h and overnight incubation (Figure S9). During incubation, the 96-well plates were kept at 4 °C in the dark, in order to minimize light exposure, as with all previous samples [33]. However, it was found that it was not possible to obtain FTIR spectra of the samples, because of the spectral background caused by the presence of HEPES.

To overcome the masking effect of the HEPES buffer on the FTIR spectra, phosphate buffer (pH 7.7) was used instead. The pH of the solution was not further adjusted, as it remained stable after the addition of Cys and 3-MPA, showing better buffering capacity than the HEPES buffer. In contrast to the thiol compounds, the SeCyst solution spectra changed over six days, while the pH of the solution increased to 9.2 immediately after the addition of the SeCyst to the AuNPs solutions, indicating loss of the buffering capacity of HEPES. The band maximum is red shifted and showed broadening of the absorbance SPR band with incubation time (Figure S10). This phenomenon could be explained by changes in the ionic strength of the solution, caused by the pH changes after the addition of L-selenocystine [41,48]. It is noteworthy that the changes in the spectra of the solutions prepared with the different ratios of SeCyst were similar. The observed broadening of the SPR band noticeable overnight suggest that under the experimental conditions the functionalized AuNPs aggregate and continue to do so over six days [48].

Since the presence of the buffers did not prevent the changes in the SPR band in the SeCyst solution, the compounds were dissolved in deionized water and the pH was adjusted to approximately 10 (Cys pH 10.80; 3-MPA pH 10.95; SeCyst pH 10.21) using 2 M NaOH in order to obtain conditions under which all three compounds can be used to prepare functionalized AuNPs. The UV-vis spectra of Cys acquired after 2 h and 4 days of incubation showed good stability for the Cys-AuNPs solutions

at all ratios with no remarkable changes in the SPR band. In contrast, the 3-MPA-AuNPs displayed physical precipitation, color change of the solution and peak broadening at 2:1 and higher ratios of the functionalizing compounds (Figure S11). Therefore, the optimum ratio of functionalizing agent/AuNPs used for subsequent experiments in terms of the stability of the solution was the 1:2 ratio for all compounds. The choice of the pH value was based on the fact that at pH 10 the percentage of the thiolate anion would be higher than the undissociated thiol for both cysteamine and 3-mercaptopropionic acid. The two compounds are characterized by pKa values of 8.35 and 4.34, respectively [50]. The pH value of the environment plays an important role in the formation of the Au-S bond, as the adsorption of thiol onto the gold surface starts with physisorption of the SH group, followed by the chemisorption and the cleavage of the S-H bond. The formation of the Au-S bond results from the deprotonation of the thiol group and the formation of thiolate radicals [51,52]. In addition, at higher pH values it has been suggested that the presence of more thiolate anions shifts the Au-S bond from a coordinate bond to a stronger covalent bond [53]. Under these conditions, the peak maximum of the SPR bands obtained for the three compounds were stable, with slight broadening of the bands between 600 and 800 nm, after 2 h and overnight incubation, indicating that the reaction was complete after 2 h with limited aggregation of the particles (Figure 1).
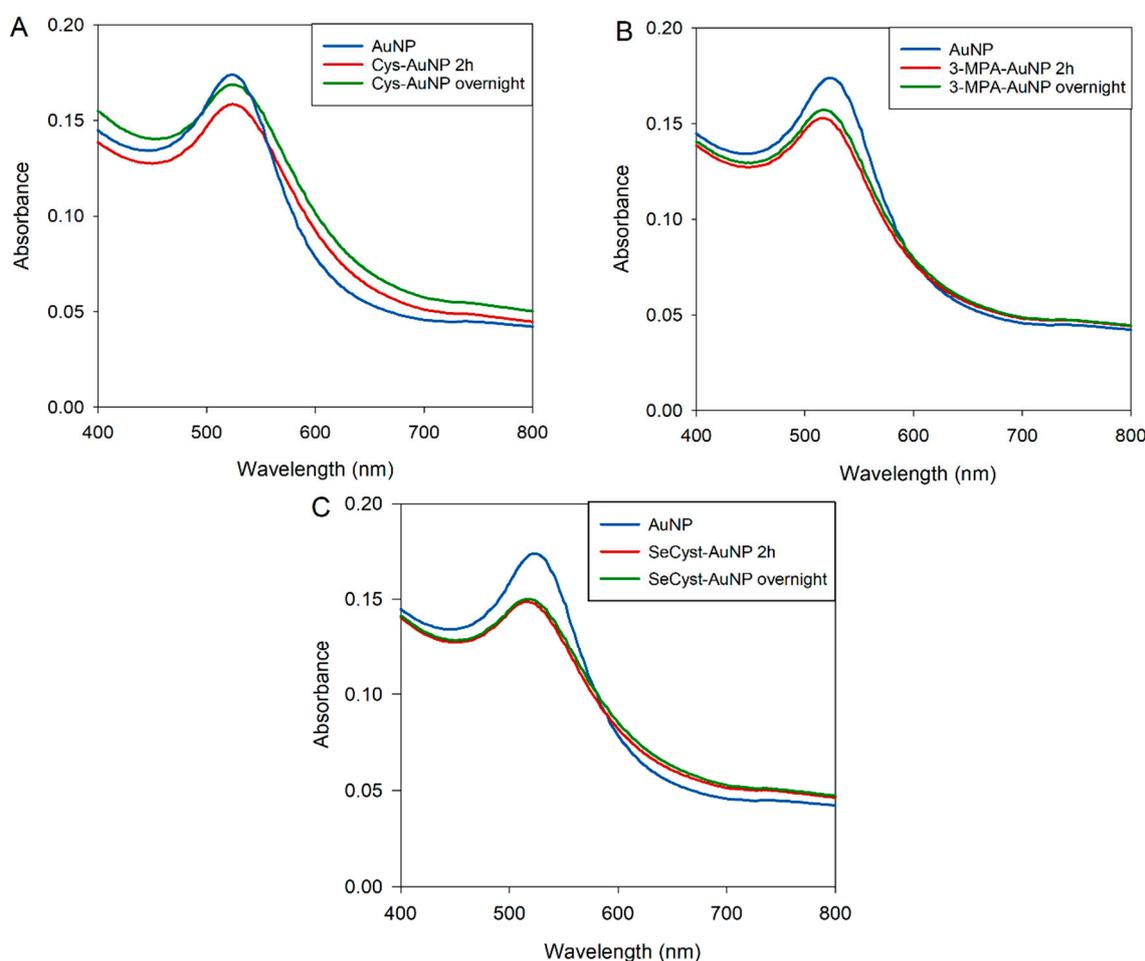

Figure 1. UV-vis spectra for stability assessment of (**A**) Cys-AuNP, (**B**) 3-MPA-AuNP, and (**C**) SeCyst-AuNP in water at 1:2 ratio after 2 h and overnight incubation, at approximately pH 10.

3.3. Functionalization of AuNPs

The optimum conditions developed above were applied for the functionalization of the purchased and synthesized nanoparticles. The conditions were kept the same throughout all experiments using

both types of AuNPs, to ensure that any discrepancy in the observations was not caused by differences in the methods that were followed.

3.3.1. Characterization of Capped-AuNPs by FTIR

To investigate the functionalization of the AuNPs with the two thiol-containing compounds, ATR-FTIR spectroscopy was deployed (Tables S3 and S4). Regarding the modification using Cys, the spectrum of cysteamine solution (pH 5.9) without pH adjustment was obtained as a reference for the v(S-H) stretching vibrational mode, which is identified at 2562 cm^{-1} (Figure S12D). This peak is absent from the spectrum of cysteamine solution (pH 10.8) and from the Cys-AuNP spectrum, due to the deprotonation of the bond and the possible Au-S bond formation, respectively. The C-S bond peak present at 700 cm^{-1} (Figure S12A), was shifted to lower wavenumbers 672 and 653 cm^{-1}, respectively for the Cys-AuNP in the synthesized and purchased samples, while it was also slightly more intense [23]. Additionally, the peaks at 1664 or 1645 cm^{-1} belonging to v_{asym}(COO$^-$) stretching, and at 1059 or 1060 cm^{-1} corresponding to v(C-O)$_{alch}$ stretching, appearing in both the Cys-AuNP spectra but were not present in the pure cysteamine spectrum, and could be associated with either citrate or the presence of α-ketoglutaric acid in the synthesized and purchased AuNP samples, respectively (Figure S12B,C) [45]. Peaks belonging to the phosphate buffer used for one of the washes were identified in both Cys-AuNP spectra (975 cm^{-1}).

Regarding the functionalization with 3-MPA, the spectrum of 3-MPA solution (pH 4.1) without pH adjustment was also obtained as a reference for the v(S-H) stretching vibrational mode, which is identified at 2567 cm^{-1} (Figure S13D). This peak was not identified in the spectrum of 3-MPA solution (pH 10.95) and in the 3-MPA-AuNP spectra, due to the deprotonation of the bond and the possible Au-S bond formation, respectively. The C-S bond peak present at 664 cm^{-1} in (Figure S13A), was slightly shifted to 680 and 660 cm^{-1} and appeared more intense when synthesized and purchased gold nanoparticles were used to produce 3_MPA-AuNP samples, respectively [23]. Similarly to the cysteamine containing samples, peaks at 1064 or 1062 cm^{-1} belonging to v_{asy}(C-O) vibrations, for the synthesized and purchased 3-MPA-AuNPs respectively, could only be attributed to entities present in either of the AuNP solutions, as they were not identified in the 3-MPA solution (Figure S13B,C). These vibrations could belong to either citrate or ketoglutarate COO- groups [44,45].

The peak assignments for the L-selenocystine containing samples are presented in Table S5. Various carbon containing bonds have been identified, along with a peak at approximately 970 cm^{-1}, present because of the phosphate buffer wash. In contrast to the thiolate compounds mentioned above, the peaks associated with Se are not always detected with FTIR spectroscopy, due to the low wavenumbers at which they appear. As with the two previous functionalizing agents, peaks at 1660 and 1679 cm^{-1} were identified in the synthesized and purchased SeCyst-containing AuNPs respectively, that were not present in the SeCyst solution, and which indicate the presence of COO- groups originating from moieties in the AuNP solutions (Figure S14B,C) [45]. According to a previous study [54], the stretching v(C-Se) peak was found at approximately 280 cm^{-1}, while the δ(CSeSe)$_{sym}$ and δ(CSeSe)$_{asym}$ bending vibrational mode were found at 221 cm^{-1} and at 178 cm^{-1}, respectively. These peaks could not be identified here, as a result of poor signal-to-noise measurements below 650 cm^{-1} (Figure S14). These bands could be better detected using Raman spectroscopy [36]. Alternatively, in order to provide evidence of the association of the AuNPs with SeCyst, TEM was used.

3.3.2. Characterization of the Capped-AuNPs by TEM

Imaging using TEM only provided evidence of the metallic core, not the presence of Cys, 3-MPA or SeCyst, and the sizes across the functionalized AuNPs were within the error of the core nanoparticles measured prior to functionalization (Figures S15 and S16). It was difficult to directly image surface coatings on the nanoparticles due to a combination of reasons; including the amount or density of coating relative to the nanoparticles, and the potential electron beam sensitivity of organic-based coatings. Imaging did however confirm the crystalline nature of the AuNP cores.

In order to detect the presence of the tethered functional groups on the surface of the AuNPs, energy dispersive X-ray (EDX) spectroscopy combined with high angle annular dark field scanning TEM (HAADF STEM) was performed. Evidence provided by EDX measurements clearly suggested the close association of Se with the surface of gold for both types of AuNPs, a possible indication of the presence of a self-assembled monolayer (Figures S17 and S18). In addition to the Au signal, Se signal was also identified when the synthesized AuNPs were used, both in mapping and the spectrum summed from the area analyzed (Figure 2).
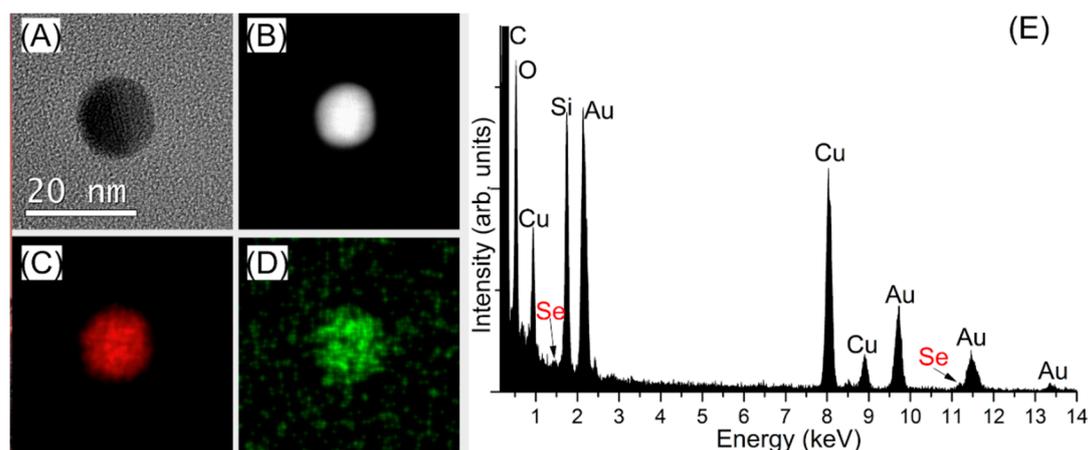
Figure 2. Analysis of Se-AuNPs using the synthesized nanoparticles, confirming the successful functionalization with SeCyst (**A**) TEM image (**B**) HAADF STEM image (**C**) Au EDX map (**D**) Se EDX map (**E**) EDX spectrum from the analyzed area, with both Au Mα and Se Lα signals (C, O, Si and Cu may be from the supporting TEM grid and carbon film).

Similar results were obtained for the purchased SeCyst-AuNPs. The EDX maps was produced using the Au Mα edge and the Se Lα edge, which are of significant different energies (2.12 keV and 1.38 keV respectively; the Se Kα edge overlaps with part of the Au Lα edge). This EDX analysis therefore suggested the presence of Se in addition to that of Au in the Se-AuNP sample, confirming the successful modification of the NPs using SeCyst and the probable formation of Au-Se bonds. Analysis of the size of the regions associated with each element were within the size range detailed above, therefore indicating either a very small coating or one which was very closely associated with the nanoparticle.

Complications arose in the EDX analysis of the Cys- and 3-MPA-functionalized samples as the signals for Au and S are very close in energy (Au Mα 2.12 keV and S Kα 2.01 keV). These edges are within the energy resolution regularly quoted for EDX spectroscopy (~0.12 keV), and it is expected that it is only possible to identify both gold and sulfur in systems with significant amounts of sulfur relative to gold, and with identification of further Au signals (such as Au Lα at 9.63 keV) and a change in the relative peak heights of the low energy peaks. It was not possible to confidently measure S by EDX spectroscopy in the Cys- or 3-MPA-AuNPs as no sulfur signal was distinguishable from the overlapping gold signal (presence of Au confirmed from additional signals), presumably due to the low concentration of S present in the system. This was further confirmed through the use of electron energy loss spectroscopy (EELS), where again no signal was detected indicating a low concentration of the element adsorbed on the gold surface. However, when compared to the Se results (Figure 2E—Very small peaks), which were collected via successive EDX scans, the lack of S signal is not surprising from either technique due to low concentrations and overlapping signals.

3.3.3. Characterization of Capped-AuNPs by UV-Visible Spectroscopy

UV-vis spectra for both purchased and synthesized capped-AuNPs were obtained (Figure 3). When using the synthesized AuNPs (Figure 3A), the SPR bands of the 3-MPA-AuNPs and the

SeCyst-AuNPs were found to blue and red shift (Table 2). The shift in the band maximum could be attributed to changes in the dielectric constant on the surface of the nanoparticles, as a result of their functionalization. Both blue and red shifts have been previously described after the binding of various surfactants, which lead to changes in the dielectric constant of gold nanoparticle solutions. However, whereas the absorption spectrum of the SPR band from the 3-MPA-AuNPs solution match that of the original AuNPs, that for the SeCyst-AuNPs showed band broadening between 550–700 nm, with accompanying color change from pink to lighter pink (Figure 3A). The band broadening could be associated with aggregation of the functionalized AuNPs [48].
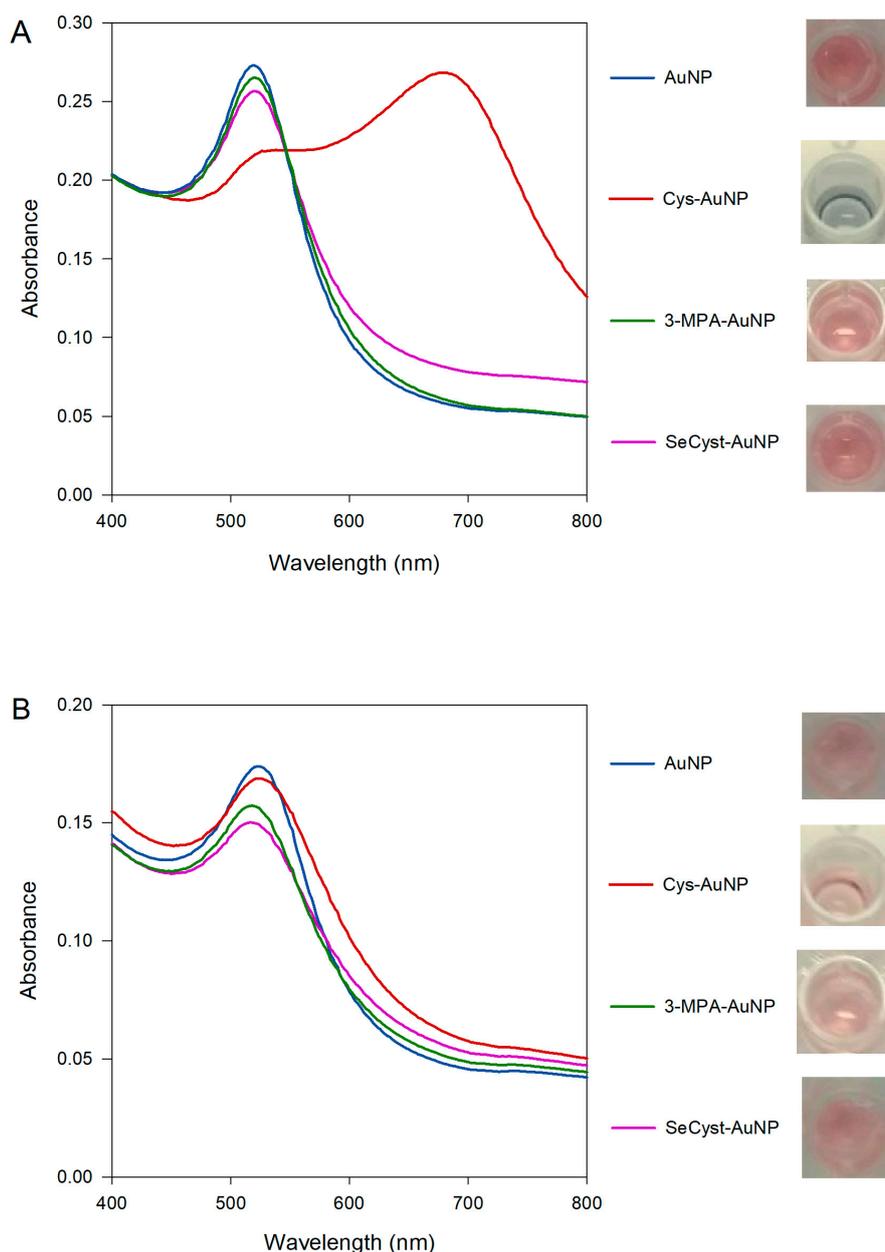

Figure 3. Comparison of the UV-vis spectra and physical appearance of the (**A**) synthesized and (**B**) purchased AuNPs stabilized by citrate and functionalized with Cys, 3-MPA and SeCyst, respectively at pH of approximately 10.

Table 2. Comparison of the SPR band λ_{max} values of synthesized and purchased AuNPs stabilized by citrate and functionalized with Cys, 3-MPA and SeCyst, respectively at pH of approximately 10.

Synthesized AuNPs	Wavelength (nm)	Purchased AuNPs	Wavelength (nm)
Cit-AuNP	520	Cit-AuNP	524
Cys-AuNP	538, 678	Cys-AuNP	525
3-MPA-AuNP	518	3-MPA-AuNP	517
SeCyst-AuNP	524	SeCyst-AuNP	516

The Cys-AuNP spectrum shows a different profile compared to the other spectra, with two SPR bands present. This phenomenon occurs when the nanoparticles are no longer regarded as having independent spherical geometry; they are too close to each other such that the localized surface plasmon resonance in the transverse and longitudinal directions overlap, thus the behavior of the AuNPs for all intents and purposes can no longer be ascribed to spherical particles. The first band is due to the transverse plasmon resonance (538 nm), and the second band, further red shift, is the longitudinal plasmon resonance band (678 nm). In this instance, the presence of two bands in combination with the change of color from red to deep blue can be explained by aggregation of the functionalized AuNPs, as a result of cross-linking of the functional groups and other citrate or α-ketoglutaric acid molecules present in the samples.

In contrast, the spectra of the functionalized purchased AuNPs show small variations with both red (Cys-AuNP) and blue shift (3-MPA-AuNP, SeCyst-AuNP) bands (Figure 3B). This is indicative of changes in the refractive index around the particles, resulting from the functionalization of the AuNPs [55]. Despite the changes in the absorption maximum, very slight color changes were observed. Only in the case of 3-MPA and SeCyst-AuNPs did the color of the solutions change from pink to lighter pink. It would be informative to rationalize the results of the experiments with reference to the structure of the functional groups in Cys, 3-MPA, and SeCyst, respectively, and the nature of the citrate-stabilized AuNPs. A good starting point would be to compare the behavior of the AuNPs functionalized with Cys and 3-MPA, since the former is amine- and the latter is carboxylic acid-terminated but with the same chain length and a thiol head group. Functionalization of synthesized AuNPs with Cys causes aggregation of the particles with the appearance of two bands at 538 and 678 nm (see Figure 3A). Results from the ATR-FTIR and ^{1}H-NMR measurements showed, that for the synthesized AuNPs there were residual citrate and oxidation products from the reduction of gold adsorbed on the surface of the formed gold nanoparticles. Same observations were made for the AuNP solutions when either of the functionalizing agents were used, indicative of the co-existence of citrate anions or α-ketoglutaric acid molecules on the surface of the nanoparticles. This adlayer can react with the amine functional group on the cysteamine on neighboring AuNPs resulting in aggregation of the particles. Comparison between the spectra generated by the synthesized and purchased AuNPs functionalized with Cys, denotes a major difference in the extent of band broadening. In this instance, careful interpretation of these results is needed, as the average diameter of the purchased AuNPs is smaller than that of the synthesized solution. Consequently, changes in the absorption spectra were less pronounced and the aggregation factor, area under the peak between 600–800 nm, was smaller when the purchased AuNPs were used. However, the effect of size alone cannot account for the reduced broadening observed when purchased AuNPs were employed. The presence of different carboxylate-containing species, those being citrate and α-ketoglutaric acid, or α-ketoglutaric acid alone adsorbed on the surface of AuNPs could be the factor limiting the extent of aggregation in the two types of AuNPs. Indeed, the difference in behavior when the purchased AuNPs with no detectable citrate was used for similar experiments provides confirmation of its role in affecting the aggregation of the AuNPs. The spectral features of AuNPs functionalized with 3-MPA, which has a fully ionized terminal carboxylic group at pH 10, show small blue shift of the SPR band maximum of 2 and 3 nm in the purchased and synthesized

solutions, respectively. An indication that electrostatic repulsion between the carboxylate groups keeps the 3-MPA functionalized AuNPs apart.

ʟ-Selenocystine presents an interesting example because of the presence of the amine and carboxylate groups in its structure. Based on the observations made above it would be expected that SeCyst-AuNPs would exhibit a behavior similar to cysteamine but not to the same extent. Comparing the aggregation factors, area under the band between 600–800 nm, clearly showed that there was less aggregation when the SeCyst-AuNPs were produced compared to the Cys-AuNPs, because of the fewer amine groups on ʟ-selenocystine. Despite the slight difference in strength of the Au-Se and the Au-S bonds not all of the citrate was dislodged from the surface of the gold nanoparticles as the selenium SAM is formed, as suggested by the ATR-FTIR data. The evidence presented here indicates that citrate and other carboxylate-containing species residues are not easily displaced from the surface of gold nanoparticles, in accordance with previous studies [34–36].

4. Conclusions

In conclusion, it is demonstrated that the characteristics of the citrate-stabilized gold nanoparticles (AuNPs), purchased or in-house synthesized, have a remarkable effect on their behavior when functionalized with alkanethiolates (cysteamine and 3-mercaptopropionic acid) or alkanediselenolate (ʟ-selenocystine). All three compounds functionalized AuNPs rapidly, in less than 2 h, when the pH of the solution was approximately 10. Under the conditions used to prepare and functionalize the in-house synthesized and purchased AuNPs, neither the thiolates nor the diselenide could completely dislodge the adsorbed carboxylate group-bearing moieties from the surface of the AuNPs. As a result, the residual negatively charged citrate or α-ketoglutaric acid ions interact with the amines on either neighboring cysteamine or ʟ-selenocystine functionalized AuNPs resulting in aggregation of the nanoparticles. As supported by UV-vis and FTIR data, the behavior of the synthesized and purchased AuNPs is different, owing to the presence of detected adsorbed citrate on the surface of the AuNPs in the former. Notably, the functionalization of the AuNPs with 3-mercaptopropionic acid remained unaffected by the presence of adsorbed molecules on the surface of the nanoparticles. Not only is the colloidal solution stable because of the electrostatic repulsion between the terminal carboxylate, but also the carbonyl group can be used to bind other functional compounds suitable for sensing applications.

5. Future Research

Future work will focus on gaining better insight into the interactions between the functionalizing compounds and citrate, using X-ray photoelectron spectroscopy, ^{13}C-NMR, zeta potential and high-resolution electron transmission microscopy measurements.

References

1. Ghosh, P.; Han, G.; De, M.; Kim, C.K.; Rotello, V.M. Gold nanoparticles in delivery application. *Adv. Drug Deliv. Rev.* **2008**, *60*, 1307–1315. [CrossRef]
2. Kong, F.-Y.; Zhang, J.-W.; Li, R.-F.; Wang, Z.-X.; Wang, W.-J.; Wang, W. Unique Roles of Gold Nanoparticles in Drug Delivery, Targeting and Imaging Applications. *Molecules* **2017**, *22*, 1445. [CrossRef]
3. Li, Y.; Schluesener, H.J.; Xu, S. Gold nanoparticle-based biosensors. *Gold Bull.* **2010**, *43*, 29–41. [CrossRef]

4.	Aldewachi, H.; Chalati, T.; Woodroofe, M.N.; Bricklebank, N.; Sharrack, B.; Gardiner, P. Gold nanoparticle-based colorimetric biosensors. *Nanoscale* **2018**, *10*, 18–33. [CrossRef]

5.	Nune, S.K.; Gunda, P.; Thallapally, P.K.; Lin, Y.-Y.; Forrest, M.L.; Berkland, C.J. Nanoparticles for biomedical imaging. *Expert Opin. Drug Deliv.* **2009**, *6*, 1175–1194. [CrossRef]

6.	Wong, A.C.; Wright, D.W.; Conrad, J.A. *General Methods in Biomarker Research and Their Applications*; Springer: Dordrecht, The Netherlands, 2014; pp. 1–26.

7.	Saha, K.; Agasti, S.S.; Kim, C.; Li, X.; Rotello, V.M. Gold Nanoparticles in Chemical and Biological Sensing. *Chem. Rev.* **2012**, *112*, 2739–2779. [CrossRef]

8.	Meng, F.; Hou, N.; Jin, Z.; Sun, B.; Li, W.; Xiao, X.; Wang, C.; Li, M.; Liu, J. Sub-ppb detection of acetone using Au-modified flower-like hierarchical ZnO structures. *Sens. Actuators B Chem.* **2015**, *219*, 209–217. [CrossRef]

9.	Bagheri, S.; Yasemi, M.; Safaie-Qamsari, E.; Rashidiani, J.; Abkar, M.; Hassani, M.; Mirhosseini, S.A.; Kooshki, H. Using gold nanoparticles in diagnosis and treatment of melanoma cancer. *Artif. Cells Nanomed. Biotechnol.* **2018**, *46*, 462–471. [CrossRef]

10.	Priyadarshini, E.; Pradhan, N. Gold nanoparticles as efficient sensors in colorimetric detection of toxic metal ions: A review. *Sens. Actuators B Chem.* **2017**, *238*, 888–902. [CrossRef]

11.	Wang, C.; Yu, C. Detection of chemical pollutants in water using gold nanoparticles as sensors: A review. *Rev. Anal. Chem.* **2013**, *32*, 1–14. [CrossRef]

12.	Amendola, V.; Pilot, R.; Frasconi, M.; Maragò, O.M.; Iatì, M.A. Surface plasmon resonance in gold nanoparticles: A review. *J. Phys. Condens. Matter* **2017**, *29*, 203002. [CrossRef]

13.	Kang, B.; Austin, L.A.; El-Sayed, M.A. Observing Real-Time Molecular Event Dynamics of Apoptosis in Living Cancer Cells using Nuclear-Targeted Plasmonically Enhanced Raman Nanoprobes. *ACS Nano* **2014**, *8*, 4883–4892. [CrossRef]

14.	Love, J.C.; Estroff, L.A.; Kriebel, J.K.; Nuzzo, R.G.; Whitesides, G.M. Self-Assembled Monolayers of Thiolates on Metals as a Form of Nanotechnology. *Chem. Rev.* **2005**, *105*, 1103–1169. [CrossRef]

15.	Hermanson, G.T. *Bioconjugate Techniques*, 3rd ed.; Academic Press, Elsevier: Oxford, UK, 2013.

16.	Ivanov, M.R.; Bednar, H.R.; Haes, A.J. Investigations of the mechanism of gold nanoparticle stability and surface functionalization in capillary electrophoresis. *ACS Nano* **2009**, *3*, 386–394. [CrossRef]

17.	Turkevich, J.; Stevenson, P.C.; Hillier, J. A study of the nucleation and growth processes in the synthesis of colloidal gold. *Discuss. Faraday Soc.* **1951**, *11*, 55–75. [CrossRef]

18.	Ojea-Jiménez, I.; Romero, F.M.; Bastús, N.G.; Puntes, V.J. Small gold nanoparticles synthesized with sodium citrate and heavy water: Insights into the reaction mechanism. *Phys. Chem. C* **2010**, *114*, 1800–1804. [CrossRef]

19.	Sivaraman, S.K.; Kumar, S.; Santhanam, V.J. Monodisperse sub-10 nm gold nanoparticles by reversing the order of addition in Turkevich method—The role of chloroauric acid. *Colloid Interface Sci.* **2011**, *361*, 543–547. [CrossRef]

20.	Grabar, K.C.; Hommer, M.B.; Natan, M.J.; Freeman, R.G. Preparation and characterization of Au colloid monolayers. *Anal. Chem.* **1995**, *67*, 735–743. [CrossRef]

21.	Ahmed, S.R.; Oh, S.; Baba, R.; Zhou, H.; Hwang, S.; Lee, J.; Park, E.Y. Synthesis of Gold Nanoparticles with Buffer-Dependent Variations of Size and Morphology in Biological Buffers. *Nanoscale Res. Lett.* **2016**, *11*, 1–11. [CrossRef]

22.	Zhao, P.; Li, N.; Astruc, D. State of the art in gold nanoparticle synthesis. *Coord. Chem. Rev.* **2013**, *257*, 638–665. [CrossRef]

23.	Havaldar, D.V.; Patil, R.V.; Moholkar, D.N.; Magdum, P.S.; Vadrale, A.P.; Pawar, K.D. Differently synthesized gold nanoparticles respond differently to functionalization with L-amino acids. *Particuology* **2020**, *52*, 97–104. [CrossRef]

24.	Frens, G. Controlled Nucleation for the Regulation of the Particle Size in Monodisperse Gold Suspensions. *Nat. Phys. Sci.* **1973**, *241*, 20–22. [CrossRef]

25.	Ji, X.; Song, X.; Li, J.; Bai, Y.; Yang, W.; Peng, X.J. Size Control of Gold Nanocrystals in Citrate Reduction: The Third Role of Citrate. *Am. Chem. Soc.* **2007**, *129*, 13939–13948. [CrossRef]

26.	Rohiman, A.; Anshori, I.; Surawijaya, A.; Idris, I. Study of Colloidal Gold Synthesis Using Turkevich Method. *AIP Conf. Proc.* **2011**, *1415*, 39–42.

27.	Kim, J.-H.; Lavin, B.W.; Burnett, R.D.; Boote, B.W. Controlled synthesis of gold nanoparticles by fluorescent light irradiation. *Nanotechnology* **2011**, *22*, 285602. [CrossRef]

28. Su, C.-H.; Wu, P.-L.; Yeh, C.-S. Sonochemical Synthesis of Well-Dispersed Gold Nanoparticles at the Ice Temperature. *J. Phys. Chem. B* **2003**, *107*, 14240–14243. [CrossRef]

29. Volkert, A.A.; Subramaniam, V.; Haes, A.J. Implications of citrate concentration during the seeded growth synthesis of gold nanoparticles. *Chem. Commun.* **2011**, *47*, 478–480. [CrossRef]

30. Patungwasa, W.; Hodak, J.H. pH tunable morphology of the gold nanoparticles produced by citrate reduction. *Mater. Chem. Phys.* **2008**, *108*, 45–54. [CrossRef]

31. Dong, J.; Carpinone, P.L.; Pyrgiotakis, G.; Demokritou, P.; Moudgil, B.M. Synthesis of Precision Gold Nanoparticles Using Turkevich Method. *Kona.* **2020**, *37*, 224–232. [CrossRef]

32. Yee, C.K.; Ulman, A.; Ruiz, J.D.; Parikh, A.; White, H.; Rafailovich, M. Alkyl Selenide-and Alkyl Thiolate-Functionalized Gold Nanoparticles: Chain Packing and Bond Nature. *Langmuir* **2003**, *19*, 9450–9458. [CrossRef]

33. Romashov, L.V.; Ananikov, V.P. Self-Assembled Selenium Monolayers: From Nanotechnology to Materials Science and Adaptive Catalysis. *Chem. Eur. J.* **2013**, *19*, 17640–17660. [CrossRef] [PubMed]

34. Park, J.W.; Shumaker-Parry, J.S. Strong Resistance of Citrate Anions on Metal Nanoparticles to Desorption under Thiol Functionalization. *ACS Nano* **2015**, *9*, 1665–1682. [CrossRef] [PubMed]

35. Chong, G.; Hernandez, R.J. Adsorption Dynamics and Structure of Polycations on Citrate-Coated Gold Nanoparticles. *J. Phys. Chem. C* **2018**, *122*, 19962–19969. [CrossRef]

36. Wei, H.; Leng, W.; Song, J.; Liu, C.; Willner, M.R.; Huang, Q.; Zhou, W.; Vikesland, P.J. Real-Time Monitoring of Ligand Exchange Kinetics on Gold Nanoparticle Surfaces Enabled by Hot Spot-Normalized Surface-Enhanced Raman Scattering. *Environ. Sci. Technol.* **2019**, *53*, 575–585. [CrossRef]

37. Perera, G.S.; Athukorale, S.A.; Perez, F.; Pittman, C.U.; Zhang, D.J. Facile displacement of citrate residues from gold nanoparticle surfaces. *J Colloid Interface Sci.* **2018**, *511*, 335–343. [CrossRef]

38. Stolarczyk, E.U.; Leś, A.; Łaszcz, M.; Kubiszewski, M.; Strzempek, W.; Menaszek, E.; Fusaro, M.; Sidoryk, K.; Stolarczyk, K. The ligand exchange of citrates to thioabiraterone on gold nanoparticles for prostate cancer therapy. *Int. J. Pharm.* **2020**, *583*, 119319. [CrossRef]

39. Rani, M.; Moudgil, L.; Singh, B.; Kaushal, A.; Mittal, A.; Saini, G.S.S.; Tripathi, S.K.; Singh, G.; Kaura, A. Understanding the mechanism of replacement of citrate from the surface of gold nanoparticles by amino acids: A theoretical and experimental investigation and their biological application. *RSC Adv.* **2016**, *6*, 17373–17383. [CrossRef]

40. Link, S.; El-Sayed, M.A. Size and Temperature Dependence of the Plasmon Absorption of Colloidal Gold Nanoparticles. *J. Phys. Chem. B* **1999**, *103*, 4212–4217. [CrossRef]

41. Liz-Marzán, L.M. Tailoring Surface Plasmons through the Morphology and Assembly of Metal Nanoparticles. *Langmuir* **2006**, *22*, 32–41. [CrossRef]

42. Jain, P.K.; El-Sayed, M.A. Surface Plasmon Resonance Sensitivity of Metal Nanostructures: Physical Basis and Universal Scaling in Metal Nanoshells. *J. Phys. Chem. C* **2007**, *111*, 17451–17454. [CrossRef]

43. Doyen, M.; Bartik, K.; Bruylants, G.J. UV–Vis and NMR study of the formation of gold nanoparticles by citrate reduction: Observation of gold–citrate aggregates. *J. Colloid Interface Sci.* **2013**, *399*, 1–5. [CrossRef] [PubMed]

44. Balasubramanian, S.K.; Yang, L.; Yung, L.Y.L.; Ong, C.N.; Ong, W.Y.; Yu, L.E. Characterization, purification, and stability of gold nanoparticles. *Biomaterials* **2010**, *31*, 9023–9030. [CrossRef] [PubMed]

45. Park, J.W.; Shumaker-Parry, J.S. Structural Study of Citrate Layers on Gold Nanoparticles: Role of Intermolecular Interactions in Stabilizing Nanoparticles. *J. Am. Chem. Soc.* **2014**, *136*, 1907–1921. [CrossRef] [PubMed]

46. Kawaguchi, S.; Kitano, T.; Ito, K. Infrared and ultraviolet spectroscopic studies on intramolecular hydrogen bonding in an alternating copolymer of isobutylene and maleic acid. *Macromolecules* **1991**, *24*, 6030–6036. [CrossRef]

47. Ojea-Jiménez, I.; Puntes, V.J. Instability of Cationic Gold Nanoparticle Bioconjugates: The Role of Citrate Ions. *J. Am. Chem. Soc.* **2009**, *131*, 13320–13327. [CrossRef]

48. Link, S.; El-Sayed, M.A. Spectral Properties and Relaxation Dynamics of Surface Plasmon Electronic Oscillations in Gold and Silver Nanodots and Nanorods. *J. Phys. Chem. B* **1999**, *103*, 8410–8426. [CrossRef]

49. Shaporenko, A.; Cyganik, P.; Buck, M.; Terfort, A.; Zharnikov, M.J. Self-Assembled Monolayers of Aromatic Selenolates on Noble Metal Substrates. *J. Phys. Chem. B* **2005**, *109*, 13630–13638. [CrossRef]

50. Wall, S.B.; Oh, J.Y.; Diers, A.R.; Landar, A. Oxidative modification of proteins: An emerging mechanism of cell signaling. *Front. Physiol.* **2012**, *3*, 369. [CrossRef]

51. Tielens, F.; Santos, E.J. AuS and SH Bond Formation/Breaking during the Formation of Alkanethiol SAMs on Au(111): A Theoretical Study. *J. Phys. Chem. C* **2010**, *114*, 9444–9452. [CrossRef]

52. Kankate, L.; Turchanin, A.; Gölzhäuser, A. On the Release of Hydrogen from the S−H groups in the Formation of Self-Assembled Monolayers of Thiols. *Langmuir* **2009**, *25*, 10435–10438. [CrossRef]

53. Xue, Y.; Li, X.; Li, H.; Zhang, W. Quantifying thiol-gold interactions towards the efficient strength control. *Nat. Commun.* **2014**, *5*, 4348. [CrossRef] [PubMed]

54. Helios, K.; Pietraszko, A.; Zierkiewicz, W.; Wójtowicz, H.; Michalska, D. The crystal structure, infrared, Raman and density functional studies of bis (2-aminophenyl) diselenide. *Polyhedron* **2011**, *30*, 2466–2472. [CrossRef]

55. Underwood, S.; Mulvaney, P. Effect of the Solution Refractive Index on the Color of Gold Colloids. *Langmuir* **1994**, *10*, 3427–3430. [CrossRef]